PROCEEDINGS OF SPIE

SPIEDigitalLibrary.org/conference-proceedings-of-spie

Fusion of rat brain histology and MRI using weighted multi-image mutual information

Palm, Christoph, Penney, Graeme, Crum, William, Schnabel, Julia, Pietrzyk, Uwe, et al.

Christoph Palm, Graeme P. Penney, William R. Crum, Julia A. Schnabel, Uwe Pietrzyk, David J. Hawkes, "Fusion of rat brain histology and MRI using weighted multi-image mutual information," Proc. SPIE 6914, Medical Imaging 2008: Image Processing, 69140M (11 March 2008); doi: 10.1117/12.770605



Event: Medical Imaging, 2008, San Diego, California, United States

Fusion of Rat Brain Histology and MRI using Weighted Multi-Image Mutual Information

Christoph $Palm^{a,b}$, Graeme P. Penney^c, William R. Crum^d, Julia A. Schnabel^e, Uwe Pietrzyk^{b,f} and David J. Hawkes^a

^aCenter of Medical Image Computing (CMIC), University College London, Gower Street, London WC1E 6BT, United Kingdom;
^bInstitute of Neuroscience and Biophysics INB-3 / Medicine, Research Center Jülich, 52425 Jülich, Germany;
^cDivision of Imaging Sciences, King's College London, Strand, London WC2R 2LS, United Kingdom;
^dInstitute of Psychiatry, King's College London, De Crespigny Park, London SE5 8AF, United Kingdom;
^eDepartment of Engineering Science, University of Oxford, Parks Road, Oxford OX1 3PJ, United Kingdom;
^fDepartment of Physics, University Wuppertal, Gaussstr. 20, 42097 Wuppertal, Germany

ABSTRACT

Introduction - Fusion of histology and MRI is frequently demanded in biomedical research to study in vitro tissue properties in an in vivo reference space. Distortions and artifacts caused by cutting and staining of histological slices as well as differences in spatial resolution make even the rigid fusion a difficult task. State-of-the-art methods start with a mono-modal restacking yielding a histological pseudo-3D volume. The 3D information of the MRI reference is considered subsequently. However, consistency of the histology volume and consistency due to the corresponding MRI seem to be diametral goals. Therefore, we propose a novel fusion framework optimizing histology/histology and histology/MRI consistency at the same time finding a balance between both goals.

Method - Direct slice-to-slice correspondence even in irregularly-spaced cutting sequences is achieved by registration-based interpolation of the MRI. Introducing a weighted multi-image mutual information metric (WI), adjacent histology and corresponding MRI are taken into account at the same time. Therefore, the reconstruction of the histological volume as well as the fusion with the MRI is done in a single step.

Results - Based on two data sets with more than 110 single registrations in all, the results are evaluated quantitatively based on Tanimoto overlap measures and qualitatively showing the fused volumes. In comparison to other multi-image metrics, the reconstruction based on WI is significantly improved. We evaluated different parameter settings with emphasis on the weighting term steering the balance between intra- and inter-modality consistency.

Keywords: registration, Mutual Information, multi-modal image fusion

1. INTRODUCTION

In biomedical research small animal models are frequently used applying *in vivo* as well as *in vitro* imaging techniques. While *in vivo* approaches like MRI and PET yield consistent 3D volumes, they lack in spatial resolution compared to high resolution *in vitro* images. Histology and autoradiographs have high in plane resolution but as they are based on cut slices they lose their 3D relationship. They are further affected by

Further author information:

C. Palm: E-mail: ch.palm@fz-juelich.de, Telephone: +49 (0)2461 61 4774

Medical Imaging 2008: Image Processing, edited by Joseph M. Reinhardt, Josien P. W. Pluim, Proc. of SPIE Vol. 6914, 69140M, (2008) 1605-7422/08/\$18 · doi: 10.1117/12.770605

Proc. of SPIE Vol. 6914 69140M-1

artifacts like tears, missing parts or nonlinear distortions caused by cutting and staining. To study *in vitro* tissue properties in an individual *in vivo* anatomical reference space and allow for 3D shape characterisation of brain structures, consistent fusion of multi-modality data is mandatory.

In this paper, we focus on the fusion of rat brain histology and MRI, which is a two-step problem. First, histology images are rigidly registered with corresponding MRI slices resulting in a histology volume. Secondly, pre-registered histologies are non-rigidly registered to MRI slices to correct at least distortions while ignoring artifacts. Here, we present our solution for the first step as a prerequisite for the second one.

Most of the automatic methods for 3D reconstruction of a series of 2D slices make no use of a 3D reference (see e.g. Nikou et al., Ourselin et al. and Pietryzk et al.). They base either on extrinsic fiducial markers, intrinsic features like landmarks and contours, principal axes or image intensities. Only the intensity-based approaches are relevant for this application, since artifacts like missing parts and frayed out borders render other approaches impractical.

However, only a 3D reference ensures general shape correctness of the resulting volume. Solutions refering to such an *in vivo* reference are proposed with application to human basal ganglia⁸ and more recently for autoradiography/MRI of monkey brains and for histology/MRI of mouse brains.^{9,10}

All three approaches start without using the reference volume by restacking the *in vitro* slices mono-modally. This holds the problem of error propagation, i.e. misregistration of one image causes all subsequent images to be misregistered as well. These misregistrations are corrected by changing parameters and rerunning the registration process for misregistered images.⁹ A graph-based reconstruction is also proposed to eliminate slices which cause large registration errors.¹⁰ Subsequently, a 3D registration of the pseudo-*in vitro* volume and the *in vivo* volume is applied, first rigidly then affine to correct for different cutting planes.^{9,10} However, stopping there ignores the curved shape of biological objects in 3D.⁹

To make use of the 3D structure of the genuine 3D volume, a sequence of 2D registrations is performed with an *in vitro* image as source and a corresponding *in vivo* slice as target. To avoid losing the coherence that has already been achieved between adjacent *in vitro* images, the transformations induced by the multi-modal registrations are smoothed in the Z-direction.^{9, 10} This framework of 3D registration, 2D multi-modal registration and transformation smoothing is iterated in a *fusion loop*.⁹

We learn from these approaches, that mono-modal restacking of histologic images is highly error-prone and that there is a gap between coherence of adjacent histologic slices and coherence between histology and MRI. Therefore, we propose to fuse both of these steps together: the mono-modal registration (adjacent histological slices) step and the multi-modal registration (histology/MRI slices) step. For this, we introduce a weighted multi-image similarity metric based on mutual information. The term *multi-image* is used in the sense of *multi-target-image*. In our case, for each histological image two target images are at hand: the corresponding MRI slice and the adjacent histological image. A weighting factor controls the impact of histology or MRI information and, hence, the impact of the associated coherence goals.

2. IMAGE MATERIAL

The images used in this work are part of an ongoing study, where a cerebral abscess in two CDF Fisher rat brains was artificially induced. The MRI scan was performed using a small animal research scanner with a UnityInova console (Varian, Palo Alto, USA), 9.4 Tesla magnet, 21cm core bore size, surface coil and a gradient magnitude of 270 mT/m. The T2 weighted spin-echo sequence (TE=24ms) resulted in 40 slices of 256×256 pixels with a resolution of $0.117 \times 0.117 \times 0.5mm$ for each data set.

After sacrificing the rat, the brain was removed and frozen in -50 °C isopentan. Then, it was cut into $20\mu m$ thick coronal slices using a cryostat microtome. To allow high throughput not all histological slices are processed further. Instead, on average every 10th slice was placed on a glass plate for subsequent staining with toluidin blue. However, if a slice to be imaged had been distorted too much, it was discarded and the next suitable slice was used in its place. Therefore, in general the histology stack shows non-equidistant gaps with an average gap size of $180\mu m$ varying between $140\mu m$ and $260\mu m$. In total, 89 slices for the first and and 28 for the second data set were captured using a stereo microscope neolumar (Zeiss, Jena, Germany) with a connected color camera (Canon, Tokyo, Japan) resulting in a spatial resolution of 3072×2304 pixels of $6\mu m^2$ size.

3. FUSION OF HISTOLOGY AND MRI

At first sight the registration between histology section and MRI would appear to be rather straightforward with a large number of potential solutions available in the literature (see e.g. Pluim et al.¹¹). Looking closer, however, there are many problems to be resolved even in the rigid body case: Precise *image correspondence* is hard to achieve due to the large difference in slice thickness between histology and MRI, differing by a factor of ten, and additionally non-equidistant gaps within the histology stack (see Sec. 2). The spatial *image resolution* of histologies exceeds those of MRI approximately by a factor of 20 resulting in less partial volume effects. Histogram-based similarity measures like mutual information face the problem of poor statistics due to the low number of corresponding MRI voxels. The *image content* of histologies differ from MRIs as a result of the removal of the skull and the subsequent staining process. Although in principle both modalities can be seen as slice-based, the *cutting plane* may vary.

We propose the following fusion framework to solve these issues. First, the high sampling of histology in the Z-direction is simulated for the MRI data by applying registration-based interpolation. ¹² Then, the irregularity of the sampling gaps within the histology sequence is propagated to the MRI volume yielding a slice-to-slice correspondence of both data sets (Figs. 1, 2). Secondly, histology and MRI are registered slice-by-slice using the corresponding MRI slice and the preregistered adjacent histological image as targets simultaneously (Fig. 3). The supplementory information of both modalities smooths the feature space yielding improving robustness. The implementation of the novel weighted multi-image mutual information is based on B-spline Parzen windows to enhance the statistics for entropy estimation. To deal with different spatial resolutions of the two target images, we sample target and source images using a Halton sequence. ¹³ As in Malandain et al., ⁹ an affine 3D registration with histology as target follows if necessary to correct for different cutting planes.

3.1 Upsampling of MRI in the Z-direction

Obviously, effective registration depends heavily on the amount of similar image content. Due to a low MRI sampling rate in Z, in some regions morphology changes significantly from one slice to another. Therefore, the MRI volume is upsampled in Z (Fig. 1a) using a registration-based interpolation technique.¹²

In summary, a non-rigid voxel-based registration algorithm is applied to two adjacent anchor slices. In an ideal scenario, the registration is aligning these slices perfectly yielding a dense deformation field to describe the transformation. Subsequently, a parallel plane between target and source image is introduced being intersected by the deformation vectors. These intersections determine the intensities of the interpolated image at the plane position.¹²

Target resolution after upsampling equals the maximum possible Z-resolution of the histological sections. Assuming a common starting slice for both modalities and preserving the original MRI slices of $500\mu m$ thickness, gaps of $480\mu m$ size are filled with 24 interpolated slices of virtual thickness of $20\mu m$ (Fig. 2).

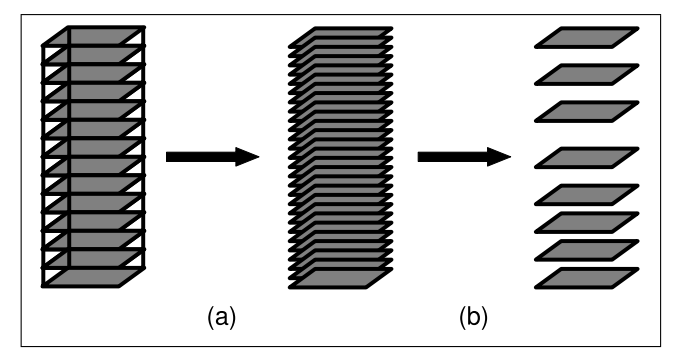


Figure 1. Registration-based interpolation of MRI data (a) to simulate high resolution in the Z-direction. The known gaps of the histological slices are introduced into the MRI data ending up with a one-to-one correspondence of histological and MRI slice.

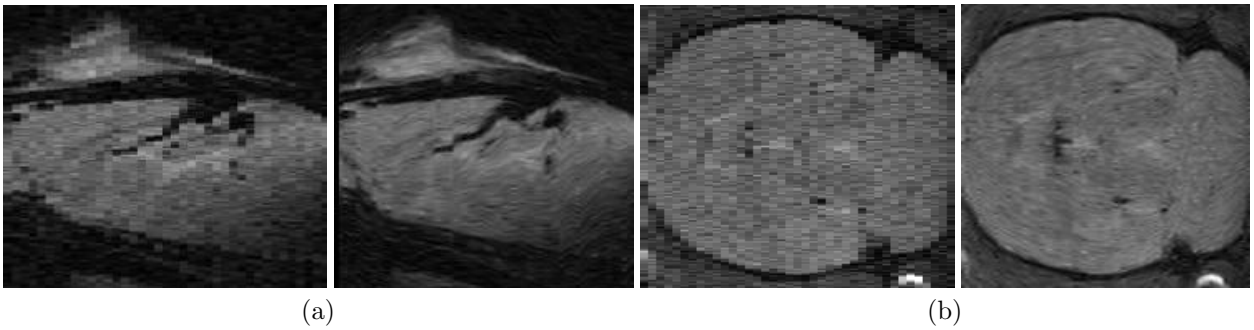


Figure 2. Sagittal (a) and horizontal view (b) for original (left) and interpolated MRI (right) after irregular sampling.

For the fusion procedure, only slices are needed which correspond to a histology. The histological images are numbered consecutively, starting with the olfactorial bulb as distinct reference. This allow adjustment of the MRI volume in the Z-direction and propagation of the irregular gaps (Fig. 1b) yielding an irregularly supersampled volume MR_n , 0 < n < N with MR_n being a coronal MRI slice and N the number of slices.

3.2 Registration of Histology and MRI

Let Π_n be the histological images which define the selection of MR_n . Adapting the notation given in Malandain et al., a rigid transformation $T_{\Pi_n \leftarrow MR_n}$ describes the mapping of points in MR_n to points in Π_n . The application of $T_{\Pi_n \leftarrow MR_n}$ to Π_n , $\Pi_n \circ T_{\Pi_n \leftarrow MR_n}$, yields a registered histology Π_n in MR geometry. A multi-image registration $\Pi_n \circ T_{\Pi_n \leftarrow MR_n, \widetilde{\Pi}_{n-1}}$ involves not only MR_n but also the previously registered $\widetilde{\Pi}_{n-1}$ as target. Choosing $R = \lfloor N/2 \rfloor$ as number of the global reference slice and starting with a multi-modal but mono-(target)-image registration (Fig. 3a), a series of multi-image registrations follows up and down the stack (Fig. 3b-d):

$$\widetilde{\mathbf{HI}}_{n} = \begin{cases}
\mathbf{HI}_{n} \circ T_{\mathbf{HI}_{n} \leftarrow \mathbf{MR}_{n}, \widetilde{\mathbf{HI}}_{n-1}}, & \text{if} \quad R < n < N, \\
\mathbf{HI}_{n} \circ T_{\mathbf{HI}_{n} \leftarrow \mathbf{MR}_{n}}, & \text{if} \quad n = R, \\
\mathbf{HI}_{n} \circ T_{\mathbf{HI}_{n} \leftarrow \mathbf{MR}_{n}, \widetilde{\mathbf{HI}}_{n+1}}, & \text{if} \quad 0 \le n < R.
\end{cases} \tag{1}$$

3.2.1 Weighted Multi-Image Mutual Information

Mutual information is a well established similarity measure for registration of multi-modal medical images.¹¹ For two images A and B, optimizing mutual information I(A, B) tends to minimize the joint entropy H(A, B) while maximizing both image entropies, H(A) and H(B): I(A, B) = H(A) + H(B) - H(A, B). There are several possibilities to generalize mutual information for more than two images.¹¹ In our application, both target images have a unified geometry due to previous registration. Therefore, the following definition is appropriate:¹⁴

$$I(A, B, C) = H(A, B) + H(C) - H(A, B, C)$$

$$= \sum_{a,b,c} p(a,b,c) \log \frac{p(a,b,c)}{p(a,b)p(c)}$$
(2)

where p(a, b, c) denotes the joint probability for intensities $a \in A$, $b \in B$ and $c \in C$, p(a, b) and p(c) analogue. The source C corresponds to HI_n , the targets A and B to MR_n and \widetilde{HI}_{n-1} , respectively, for the first case in (1). According to (3), A and B are treated as a single union target image. The major drawback of this approach is that the contribution of each target image to the final measure cannot be scaled. Particularly with regard to histology restacking, there is one target image with large differences (MRI) due to differing modalities and one target image with much smaller differences (histology) due to morphological changes. This means I(A, B, C) effectively forces C to be more similar to B than to A. This effect is so huge, that we end up with a metric which is very similar to I(B, C) for pure mono-modal restacking. To overcome this problem, weighted multi-image

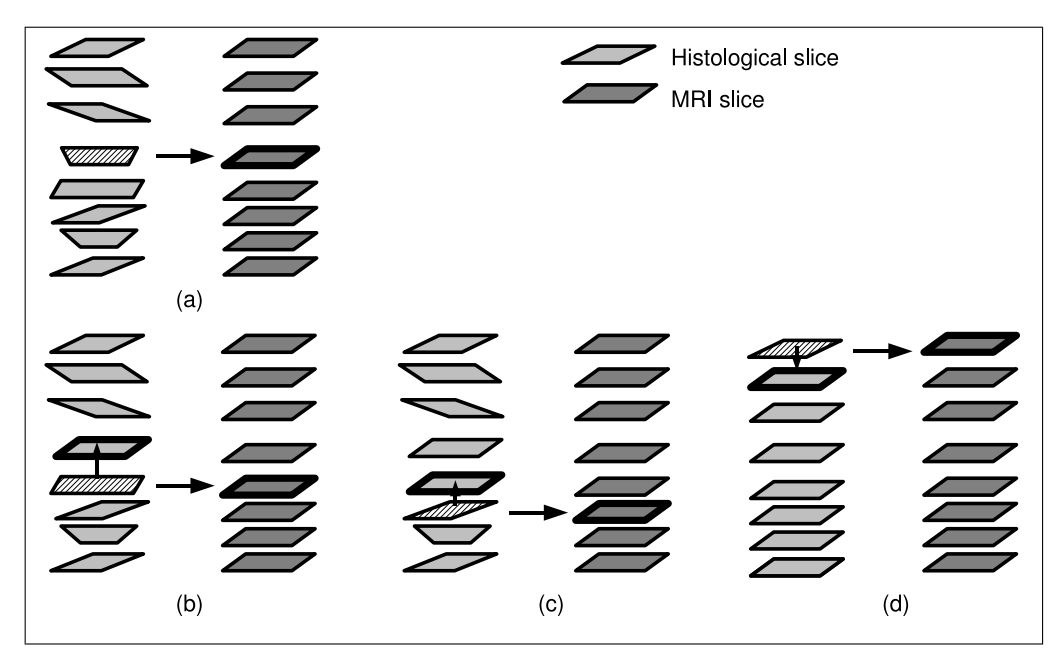


Figure 3. Schematic view of the registration framework using two targets at the same time. After initialisation registering one histological slice to the correspondent MRI slice (a) the procedure moves down (b, c) and up (d) the stack taking the MRI slice and the adjacent histology into account. The sketch shows the source image striped and the target images with a bold line.

mutual information WI with weight $\alpha \in [0:1]$ is introduced here:

$$WI(A, B, C) = \alpha H(A) + (1 - \alpha)H(B) + H(C) -\alpha H(A, C) - (1 - \alpha)H(B, C)$$

$$= \alpha \sum_{a,b,c} p(a, b, c) \log \frac{p(b)p(a, c)}{p(a)p(b, c)}$$

$$+ \sum_{a,b,c} p(a, b, c) \log \frac{p(b, c)}{p(b)p(c)}$$
(3)

Note, that WI(A, B, C) = I(A, C) is true for $\alpha = 1$ and WI(A, B, C) = I(B, C) for $\alpha = 0$. The main advantage of WI is the individual scalability of the contributions of each target to the final measure.

3.2.2 Halton Sampling

Despite the differing resolutions of both targets, for p(a,b,c) common samples are needed. WI can be implemented with joint or separate sampling of both targets. Since the histological image is physically much smaller, joint sampling implicates a masking of the MRI. To allow for uniform joint target sampling, a Halton sequence r_k is utilized.¹³ Briefly, for one dimension and for a prime basis B a sequence of rational numbers r_k with

$$r_k = B^{-L} \sum_{l=0}^{L-1} b_{L-1-l} B^l, \quad k = \sum_{l=0}^{L-1} b_l B^l, \quad L = 1 + \lfloor \log_B k \rfloor$$

 $b_l \in \{0, 1, \dots, B-1\}$, is constructed given a consecutive number of positive integers k. This sequence is characterised as low-discrepancy, i.e. it is able to cover the image domain uniformly. A further advantage is removal of the well known *grid effect* of mutual information, because the samples neither are dependent on the target nor on the source grid. Details and effects of this kind of sampling on registration can be found in Thevenaz et al.¹³

Table 1.	Experimental	results for	different	metrics and	parameter settings.

Method					Data	set 1		Data set 2		
Metric	Init.	NoS	Joint?	$\alpha_{ m opt}$	Intra	Inter	$\alpha_{ m opt}$	Intra	Inter	
\overline{I}	IC	2	yes	_	0.859	0.782	_	0.970	0.911	
	CoG	2	yes	_	0.857	0.791	_	0.970	0.914	
	CoG	4	yes	_	0.855	0.769	_	0.969	0.915	
	CoG	8	yes	_	0.860	0.785	_	0.970	0.913	
\overline{WI}	IC	2	no	0.8	0.792	0.741	0.9	0.955	0.806	
	IC.	2	yes	0.8	0.854	0.794	0.9	0.956	0.889	
	CoG	2	yes	0.8	0.878	0.810	0.9	0.967	0.913	
	CoG	4	yes	0.8	0.879	0.809	0.9	0.967	0.919	
	CoG	8	yes	0.8	0.883	0.810	0.9	0.967	0.918	

In the case of 2D multi-image mutual information, Halton sampling helps to maintain different spatial resolutions of two target images and, thus, preserving all information. Both target images are evaluated at the sample positions by means of cubic B-spline interpolation. The joint histogram is filled applying cubic B-spline Parzen windows in all directions.¹³

4. EXPERIMENTS AND RESULTS

To evaluate the novel fusion strategy using WI(A, B, C), we set up several exeriments for different parameters and compare the results to using I(A, B, C) based on two data sets. The first data set covers the whole rat brain including the cerebellum. The slices of the second data set are located only in the mid-brain, where distortions are less probable and, thus, the restacking itself is much easier.

All experiments have in common a bin size of five and ten for histograms involving MRI and histological images, respectively. The feature space is optimized using an evolutionary optimization strategy. Beside the general comparison of both similarity measures in question, our experiments include different kinds of initialization like image centre (Image Centre (IC) in Tab. 1) or centre of gravity given by the spatial distribution of image intensities (Centre of Gravity (CoG) in Tab. 1). The effect of joint or separate sampling of target images ($Joint?\ yes/no$ in Tab. 1), number of samples ($NoS \times 10000$ in Tab. 1) and weighting factor α are studied. For I only joint sampling is possible and no optimal $\alpha_{\rm opt}$ is specified. Note, that with $\alpha=0$, the very first step of mono-modal restacking 9,10 is approximated.

Quantitative results are calculated by the Tanimoto overlap measure.¹⁶ After manual labeling of the brain tissue in both modalities and comparing pairwise adjacent histologies, the mean over the whole stack yields a

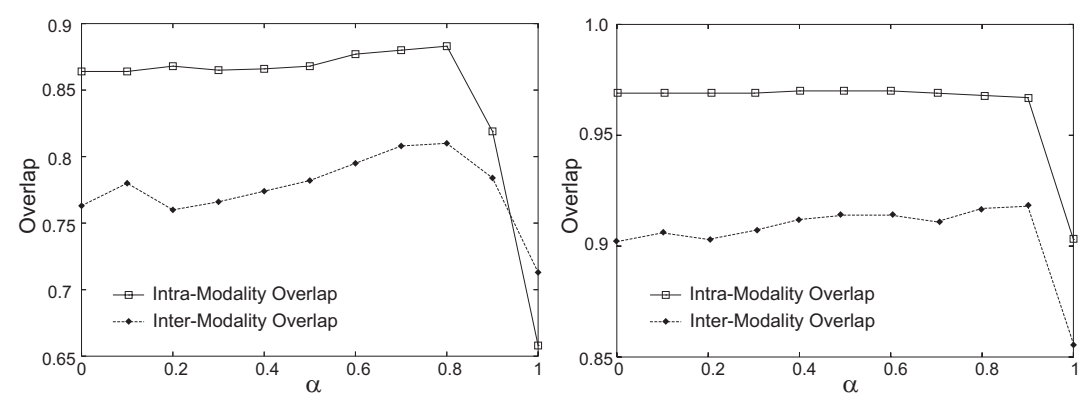


Figure 4. α -curves for intra- and inter-modality Tanimoto overlap of first (left) and second (right) data set.

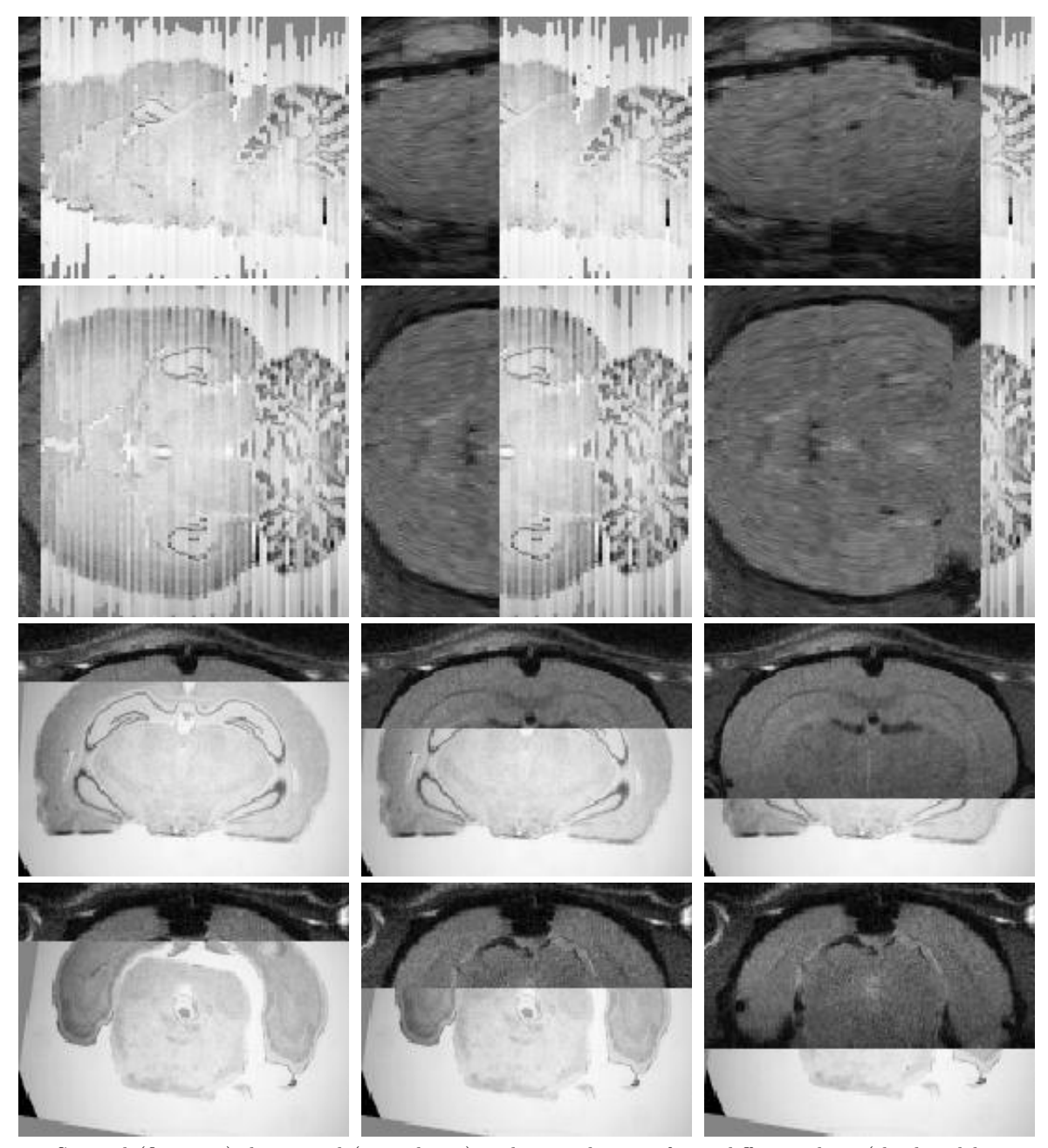


Figure 5. Sagittal (first row), horizontal (second row) and coronal view of two different slices (third and last row) for $\alpha = 0.8$ of first data set (see Tab. 1) sliding between both fused data sets.

measure of intra-modality coherence (*Intra* in Tab. 1). Comparing pairwise corresponding labels of histology and MRI slices, the corresponding mean provides an inter-modality coherence value (*Inter* in Tab. 1).

Table 1 shows the results of different experiments, which vary less regarding the second data set in comparison to the first. The reason is the differing coverage of the brain with only mid-brain parts of the second and the whole rat brain of the first data set. Taking joint sampling of both target images and initialization due to CoG rather than IC into account improved coherence values are recognisable. By increasing the numbers of samples from 20000 to 80000 the results of data set one show a small rise in intra-modality overlap and a constant or slightly falling inter-modality overlap. For data set two the intra-modality coherence is nearly constant for all

experiments, the inter-modality overlap rises. The optimum number of samples is 80000 for data set one and 40000 for data set two. α was determined empirically given the intra- and inter-modality overlap curves for 80000 joint samples and CoG initialization (Fig. 4). As α is increased the intra-modality overlap rises slightly for the first data set and staying nearly constant for the second one, but falls down rapidly reaching $\alpha = 1.0$. The inter-modality overlap curve rises more steeply and reaches an optimum at $\alpha = 0.8$ for the first and at $\alpha = 0.9$ for the second data set. The best result of the first data set is visualised in Fig. 5 showing very accurate registration even in cases of distortions for which one coronal example is given (Fig. 5, last row).

5. DISCUSSION AND CONCLUSION

In this work, a fusion framework given a histological image stack and a MRI volume is proposed. It deals with irregular gaps between adjacent histologies by upsampling the MRI in the Z-direction using registration-based interpolation yielding virtual slices of $20\mu m$ thickness. However, since the anchor slices have in fact a thickness of $500\mu m$, they suffer from partial volume effects which are not eliminated by the interpolation but carried forward to the interpolated slices. The registration is performed using a novel weighted multi-image mutual information measure allowing the adjustment of intra- and inter-modality coherence within one registration step. Therefore, parts of the complex application of a fusion loop⁹ can be avoided. An affine adjustment of differing cutting planes may follow, but was not necessary for our data.

By taking the corresponding MRI slice as well as the already registered adjacent histology into account at the same time, robustness of the fusion process increases because of complementary information of the two targets. To use low as well as high resolution targets simultaneously, Halton sampling decouples pixels and samples. The optimum coherence was achieved using a number of samples which is much higher than the number of pixels in a MRI image. Nevertheless, the improvement is small and computation time increases linearly with the number of samples.

Despite of distortions or missing parts, the histology is very accurately fused with the MRI volume for a proper adjustment of the weighting factor α . α determines the influence of one target image against the other. This was necessary, because assuming perfect registration of all three target images involved, the remaining joint entropy of histology source and MRI target is much higher than that of histology source and adjacent histology target due to the differing imaging modalities. Therefore, α plays the role of adjusting these differing baselines and the need of overweighting the MRI with $\alpha > 0.5$ could be expected. After empirical determination here, we intend to evaluate new data from this ongoing study in particular to determine the optimum α from the data directly.

ACKNOWLEDGMENTS

For this work, Christoph Palm was supported by the German Research Foundation (DFG), grant PA1595/1-1. We also thank Dagmar Salber and Anca Oros-Peusgens (Research Centre Juelich, Germany) for providing the stained rat brain histologies and MRIs, respectively.

REFERENCES

- C. Nikou, F. Heitz, A. Nehling, I. Namer, and J.-P. Armspach, "A robust statistics-based global energy function for the alignment of serially acquired autoradiographic sections," *Journal Neuroscience Methods* 124, pp. 93–102, 2003.
- 2. S. Ourselin, A. Roche, G. Subsol, X. Pennec, and N. Ayache, "Reconstructing a 3D structure form serial histologic sections," *Image Vision Computing* **19**, pp. 25–31, 2000.
- 3. U. Pietrzyk, D. Bauer, A. Vieten, A. Bauer, K.-J. Langen, K. Zilles, and C. Palm, "Creating consistent 3D multi-modality data sets from autoradiographic and histological images of the rat brain," in *IEEE Nuclear Science Symposium Conference Record*, 6, pp. 4001–4003, 2004.
- J. L. Humm, R. M. Macklis, X. Q. Lu, Y. Yang, K. Bump, B. Beresford, and L. M. Chin, "The spatial accuracy of cellular dose estimates obtained from 3D reconstructed serial tissue autoradiographs," *Physics Medicine Biology*, pp. 163–180, 1995.

- 5. S. Krinidis, C. Nikou, and I. Pitas, "Reconstruction of serially acquired slices using physics-based modeling," *IEEE Transactions Information Techniques and Biomedicine* **7**(4), pp. 394–403, 2003.
- 6. A. Rangarajan, H. Chui, S. Pappu, L. Davachi, P. S. Goldman-Rakic, and J. S. Duncan, "A robust point matching algorithm for autoradiographic alignment," *Medical Image Analysis* 4(1), pp. 379–398, 1997.
- 7. O. Schmitt, J. Modersitzki, S. Heldmann, S. Wirtz, and B. Fischer, "Image registration of sectioned brains," *International Journal of Computer Vision* **73**, pp. 5–39, June 2007.
- 8. S. Ourselin, E. Bardinet, D. Dormont, G. Malandain, A. Roche, N. Ayache, D. Tandé, K. Parain, and J. Yelnik, "Fusion of histological sections and MR images: Towards the construction of an atlas of the human basal ganglia," in *MICCAI 2001*, W. Niessen and M. Viergever, eds., pp. 743–751, Springer, 2001.
- 9. G. Malandain, E. Bardinet, K. Nelissen, and W. Vanduffel, "Fusion of autoradiographs with an MR volume using 2D and 3D linear transformations," *NeuroImage* **23**, pp. 111–127, 2004.
- P. A. Yushkevich, B. B. Avants, L. Ng, M. Hawrylycz, P. D. Burstein, H. Zhang, and J. C. Gee, "3D mouse brain reconstruction from histology using a coarse-to-fine approach," in WBIR 2006, J. P. W. Pluim, B. Likar, and F. A. Gerritsen, eds., pp. 230–237, Springer, 2006.
- 11. J. P. W. Pluim, J. B. A. Maintz, and M. A. Viergever, "Mutual-information-based registration of medical images: A survey," *IEEE Transactions Medical Imaging* **22**, pp. 986–1004, Aug. 2003.
- 12. G. P. Penney, J. A. Schnabel, D. Rueckert, M. A. Viergever, and W. J. Niessen, "Registration-based interpolation," *IEEE Transactions Medical Imaging* 23, pp. 922–926, July 2004.
- 13. P. Thévenaz, M. Bierlaire, and M. Unser, "Halton sampling for image registration based on mutual information," Sampling Theory in Signal and Image Processing, in press, 2008.
- 14. C. Studholme, D. L. G. Hill, and D. J. Hawkes, "Incorporating connected region labelling into automated image registration using mutual information," in *IEEE Proceedings MMBIA '96*, pp. 23–31, 1996.
- 15. M. Styner, C. Brechbühler, G. Székely, and G. Gerig, "Parametric estimate of intensity inhomogeneities applied to MRI," *IEEE Transactions Medical Imaging* 19, pp. 153–165, March 2000.
- 16. W. R. Crum, O. Camara, and D. Hill, "Generalized overlap measures for evaluation and validation in medical image analysis," *IEEE Transactions Medical Imaging* **25**, pp. 1451–1461, Nov. 2006.